Supporting information

Unraveling the Contributions of Internal Resistance Components in Two-Chamber Microbial Fuel Cells Using the Electrode Potential Slope Analysis

Ruggero Rossi[1], Bruce E. Logan[1]*

[1]Department of Civil and Environmental Engineering, The Pennsylvania State University, 231Q Sackett Building, University Park, PA 16802, USA

*Corresponding author: e-mail: blogan@psu.edu; phone: +1-814-863-7908; fax: +1-814-863-7304

Number of pages: 20
Number of figures: 15
Number of tables: 2

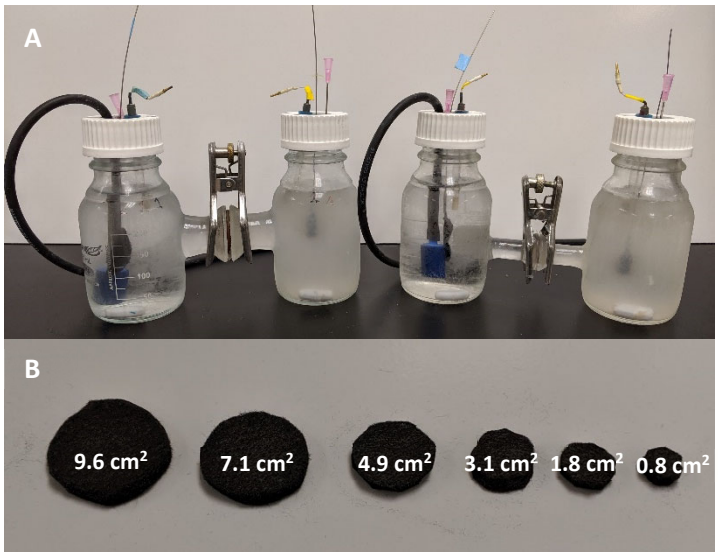

Figure S1. Photos of (A) the double chamber MFCs with different tube cross-sectional areas (LT-MFC = 4.5 cm^2 on the left; ST-MFC = 1.2 cm^2 on the right) and (B) the electrode dimensions used in polarization tests.

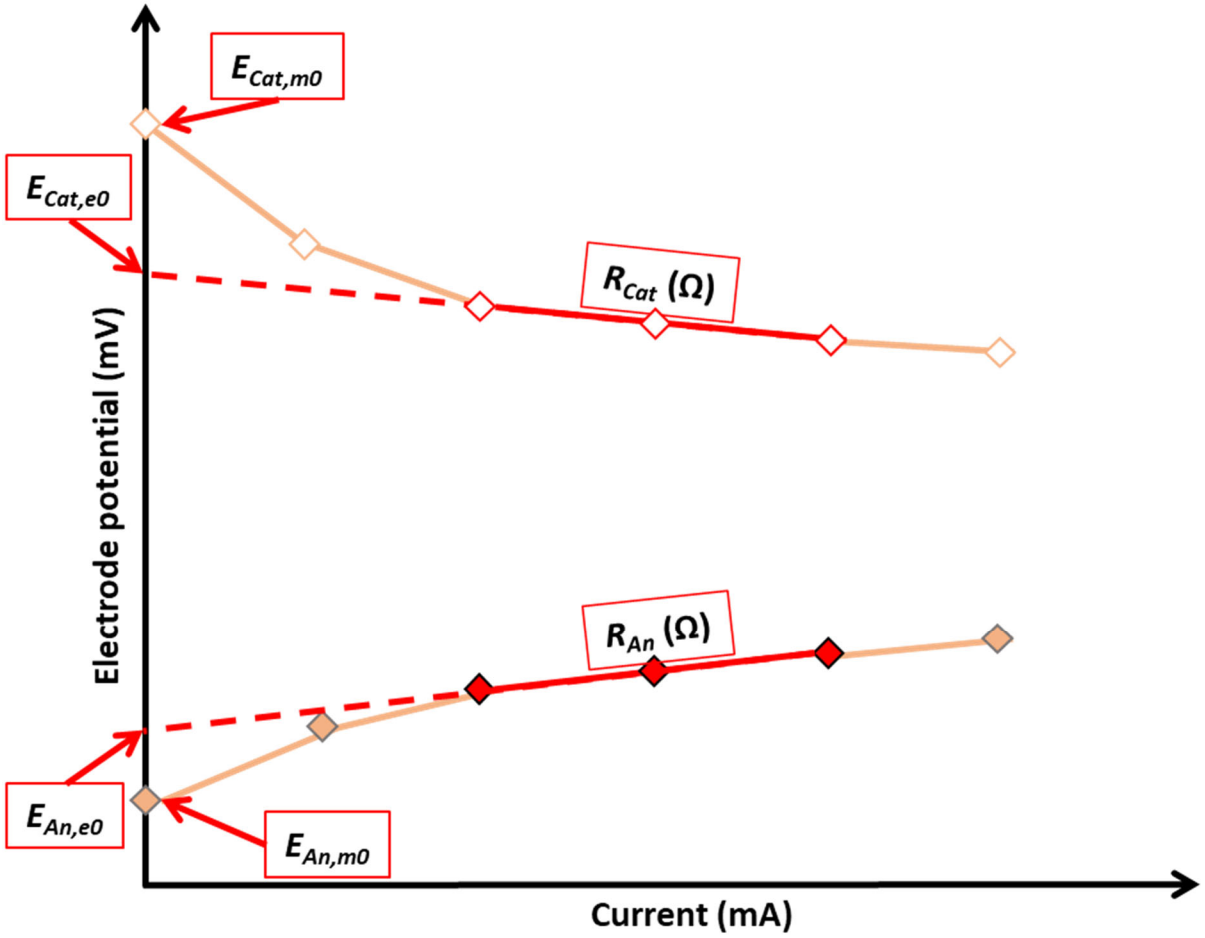

Figure S2: Schematic representation of the parameters used for the EPS analysis. $E_{Cat,m0}$ and $E_{An,m0}$ are the cathodic and anodic potential measured at open circuit condition.The red dashed lines represent the linearization that would be obtained from polarization tests, and the intercept of this line with the electrode potential axis has been used to calculate the cathodic ($E_{Cat,e0}$) and anodic ($E_{An,e0}$) experimental potential at zero current. The thick solid lines show the linearized portion of the polarization data that are used to calculate the anode (R_{An}) and cathode (R_{Cat}) resistances.

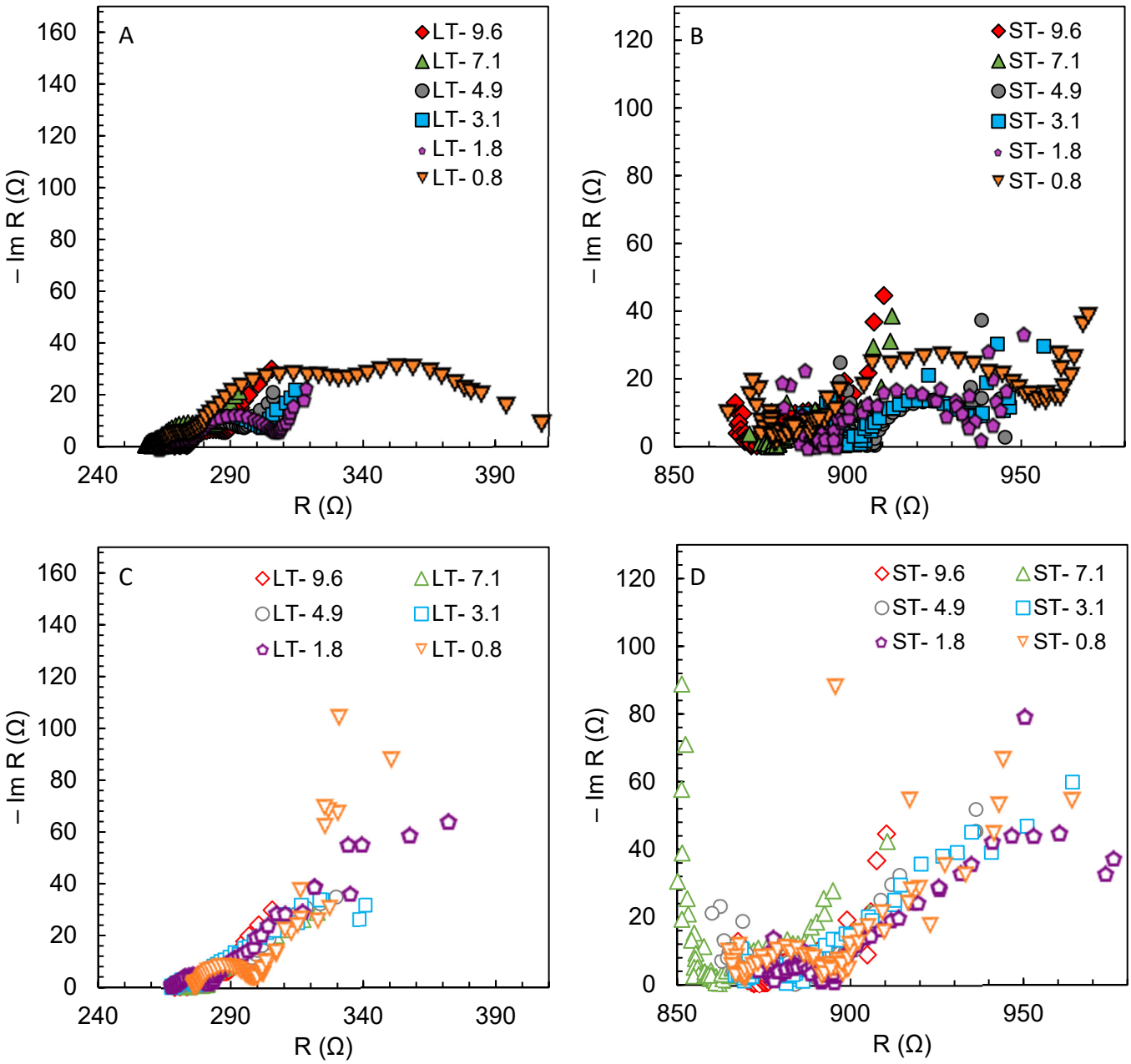

Figure S3. EIS spectra on 4.5 cm^2 tube MFC (LT) and 1.2 cm^2 tube MFC (ST) varying the (A, B) anode and (C, D) cathode projected area from 9.6 cm^2 to 0.8 cm^2.

MFC equivalent circuit. Three depressed semicircles were obtained in the Nyquist plot of the whole cell MFC for the large tube (LT- 4.5 cm^2) and small tube (ST- 1.2 cm^2) MFCs, each of them representing a distinct process (Figure S4). The first process (Q_Ω/R_Ω) was likely due to the inner porosity of the carbon materials over the electroactive region.[1,2] Previous studies have also identified this process and the correspondent capacitance with the electrochemically active biofilm.[3,4] The second process (Q_{An}/R_{An}) was the anodic electron transfer while the third process was identified with the cathodic reaction (Q_{Cat}/R_{Cat}) (Figure S4A). The spectra of the MFCs with the smaller cathode (0.8 cm^2) was modified to include a diffusion element in it, due to the mass-transfer limitations of oxygen (Figure S4B). A constant phase element (CPE, correspondent to *Q* in the circuit) was used for fitting the spectra instead of a pure capacitance. This is due to the fact that in our system the large porosity of the carbonaceous electrodes resulted in an uneven distribution of the potential and a consequent dispersion of the time constants.[4–6] This phenomenon is very common for highly porous materials, and has been extensively explained in the literature.[6–8]

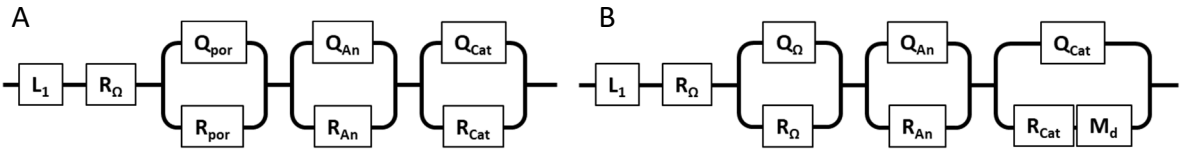

Figure S4. Equivalent circuit used to fit the impedance diagrams of the MFCs.

Table S1. Inductance, pseudocapacitance and resistance derived from fitting the EIS spectra to the equivalent circuit for the MFCs with tube area of 4.5 cm^2 (LT) and variable anode and cathode areas.

LT - 4.5 cm^2 tube

		Variable Cathode Area					Variable Anode Area				
	9.6 cm^2	7.1 cm^2	4.9 cm^2	3.1 cm^2	1.8 cm^2	0.8 cm^2	7.1 cm^2	4.9 cm^2	3.1 cm^2	1.8 cm^2	0.8 cm^2
L_1	2.5×10^{-7}	9.5×10^{-7}	8.9×10^{-7}	7.2×10^{-8}	1.5×10^{-14}	0.0	1.3×10^{-6}	1.4×10^{-6}	7.8×10^{-7}	1.7×10^{-127}	1.3×10^{-155}
R_Ω	258	273	270	268	268	276	257	267	265	263	262
Q_{por}	8.0×10^{-3}	3.5×10^{-3}	1.2×10^{-3}	7.8×10^{-4}	5.3×10^{-4}	7.5×10^{-6}	1.7×10^{-2}	6.5×10^{-3}	3.2×10^{-3}	2.3×10^{-3}	2.0×10^{-3}
α	0.31	0.47	0.56	0.65	0.65	1.00	0.32	0.44	0.44	0.49	0.51
R_{por}	8.55	8.37	11.00	10.52	15.16	1.62	6.35	6.13	9.51	13.88	20.04
Q_{An}	3.7×10^{-2}	3.9×10^{-2}	4.0×10^{-2}	5.9×10^{-2}	5.3×10^{-2}	1.0×10^{-4}	3.5×10^{-2}	2.3×10^{-2}	1.4×10^{-2}	1.0×10^{-2}	5.7×10^{-3}
α	0.94	0.92	1.00	1.00	1.00	0.86	0.89	0.83	0.81	0.85	0.91
R_{An}	12.2	15.6	12.4	9.0	15.6	20.4	18.6	23.3	30.9	32.2	54.8
Q_{Cat}	5.5×10^{-1}	3.9×10^{-1}	2.1×10^{-1}	1.1×10^{-1}	1.3×10^{-1}	1.6×10^{-2}	5.9×10^{-1}	7.6×10^{-1}	9.8×10^{-1}	8.1×10^{-1}	1.0×10^{-1}
α	0.86	0.85	0.78	0.71	0.81	0.80	0.82	0.87	0.95	0.91	1.00
R_{Cat}	87.3	73.5	98.2	101.8	150.0	153.0	90.2	84.2	76.0	92.6	62.8
R_d						282.3					
t_d						9.7					

Table S2. Inductance, pseudocapacitance and resistance derived from fitting the EIS spectra to the equivalent circuit for the MFCs with tube area of 1.2 cm^2 (ST) and variable anode and cathode areas.

ST - 1.2 cm^2 tube

		Variable Cathode Area					Variable Anode Area				
	9.6 cm^2	7.1 cm^2	4.9 cm^2	3.1 cm^2	1.8 cm^2	0.8 cm^2	7.1 cm^2	4.9 cm^2	3.1 cm^2	1.8 cm^2	0.8 cm^2
L_1	-2.0×10^{-5}	-1.8×10^{-4}	-3.7×10^{-5}	-1.9×10^{-5}	-2.1×10^{-5}	-2.0×10^{-5}	-2.2×10^{-5}	-3.8×10^{-5}	-1.8×10^{-5}	-3.5×10^{-5}	-4.5×10^{-5}
R_Ω	860	847	862	865	875	867	876	895	879	884	873
Q_{por}	1.9×10^{-3}	4.7×10^{-4}	5.3×10^{-4}	1.6×10^{-3}	6.5×10^{-4}	2.5×10^{-5}	2.7×10^{-2}	2.1×10^{-2}	1.2×10^{-3}	6.1×10^{-5}	7.3×10^{-3}
α	0.43	0.47	0.51	0.45	0.57	0.92	0.32	0.17	0.25	0.68	0.30
R_{por}	9.23	14.84	19.85	20.42	20.11	1.51	4.44	31.50	27.33	9.36	33.94
Q_{An}	3.2×10^{-2}	3.9×10^{-2}	5.1×10^{-2}	5.6×10^{-2}	5.1×10^{-2}	1.3×10^{-4}	3.2×10^{-2}	2.7×10^{-2}	1.6×10^{-2}	7.8×10^{-3}	4.8×10^{-3}
α	0.80	0.70	0.39	0.99	1.00	0.79	0.80	0.98	0.83	0.77	0.89
R_{An}	24.4	35.4	44.4	12.1	13.8	27.4	26.9	22.6	34.9	46.1	55.3
Q_{Cat}	8.4×10^{-1}	8.4×10^{-1}	3.6×10^{-1}	1.0×10^{-1}	8.1×10^{-2}	2.9×10^{-2}	1.1	1.3	9.6×10^{-1}	1.0	7.7×10^{-1}
α	1.00	1.00	0.90	0.73	0.80	0.75	1.00	1.00	1.00	1.00	1.00
R_{Cat}	86.7	79.5	118.9	141.9	118.6	140.2	129.1	143.8	133.3	119.5	117.2
R_d						202.9					
t_d						23.5					

The solution resistance (R_{Ω}) was not affected by the relative area of the electrode in both LT-MFC and ST-MFC. By decreasing the anode area the respective resistance increases while the cathode resistance was fairly stable. For example, in LT-MFC, when the anode area was reduced from 9.6 cm^2 to 0.8 cm^2, the anode resistance increased by 4×, from 12.2 Ω, to 54.8 Ω while the cathode resistance changed less than 28% (from 87.3 Ω to 62.8 Ω). The resistance associated with the cathodic reaction increased by diminishing the cathode area, for example R_{Cat} increased from 87.3 Ω to 153 Ω by reducing the cathode area from 9.6 cm^2 to 0.8 cm^2.

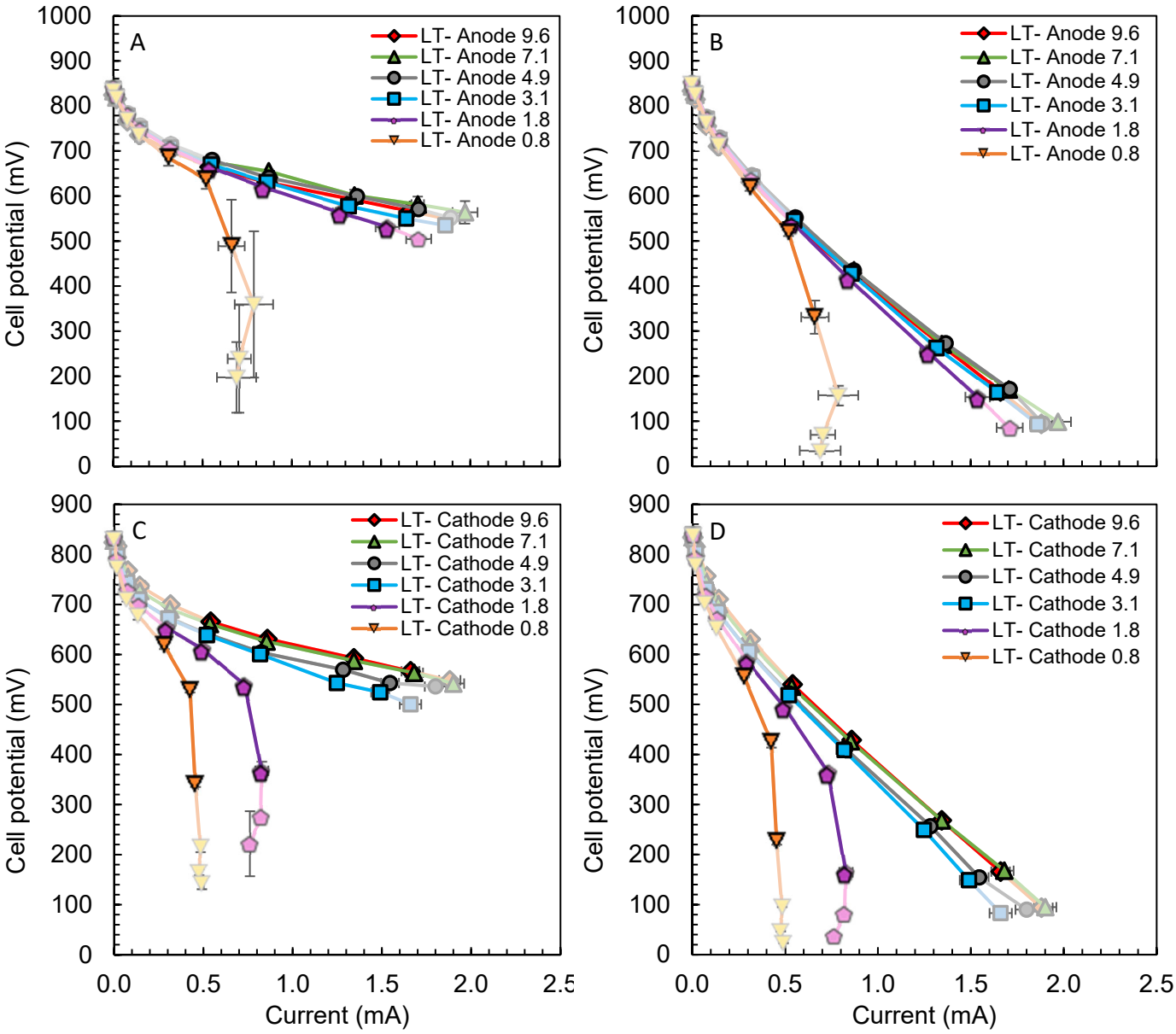

Figure S5. Polarization curves of the LT-MFC with variable (A,B) anode and (C,D) cathode electrode areas (A, C) not including the solution resistance or (B, D) including solution resistance. The thick solid lines show the linearized portion of the slopes that are used to calculate the internal resistance (R_{int}) and the internal and solution resistance ($R_{int} + R_{\Omega}$).

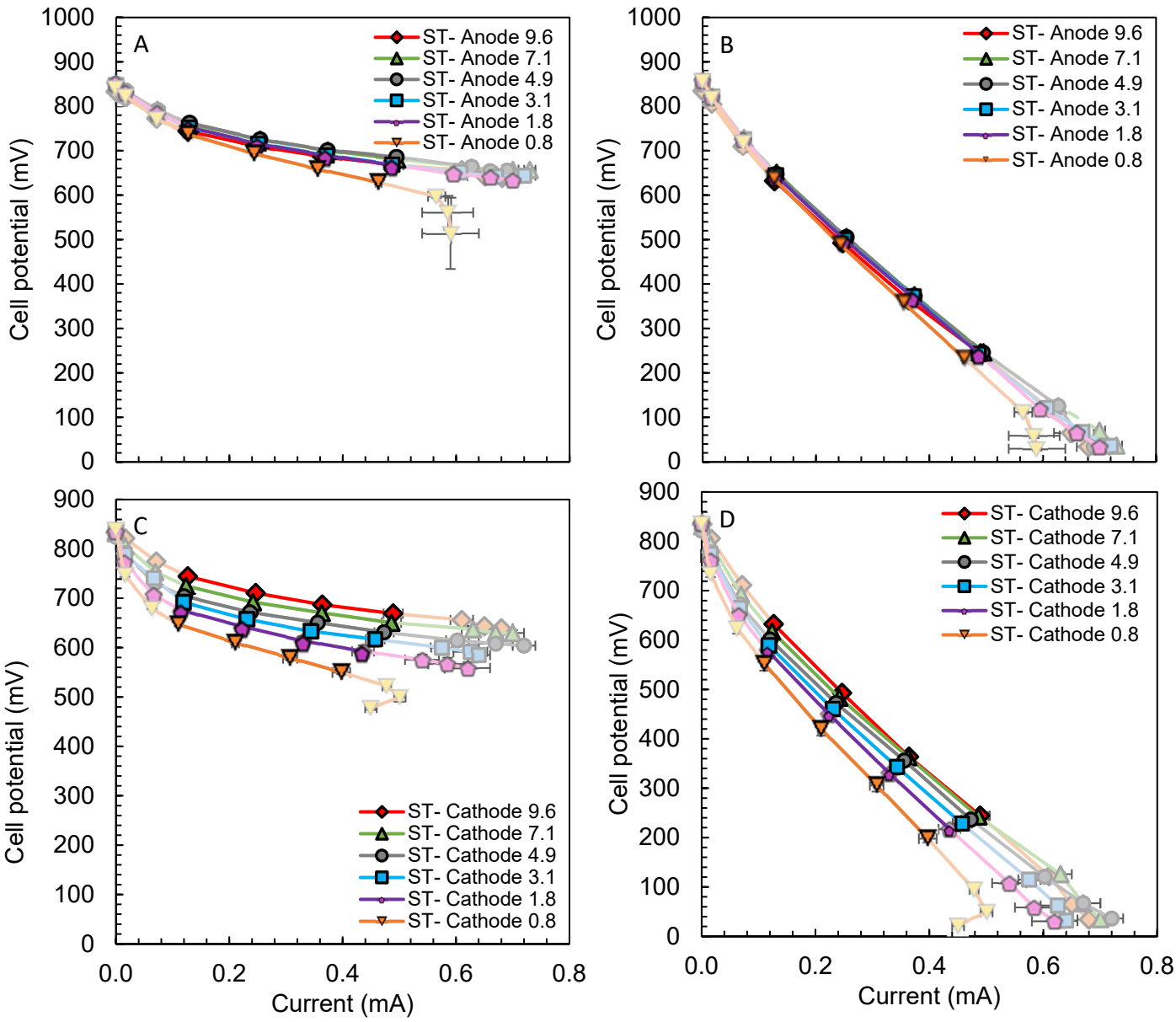

Figure S6. Polarization curves of the ST-MFC with variable (A,B) anode and (C,D) cathode electrode areas (A, C) not including the solution resistance or (B, D) including solution resistance. The thick solid lines show the linearized portion of the slopes that are used to calculate the internal resistance (R_{int}) and the internal and solution resistance ($R_{int} + R_{\Omega}$).

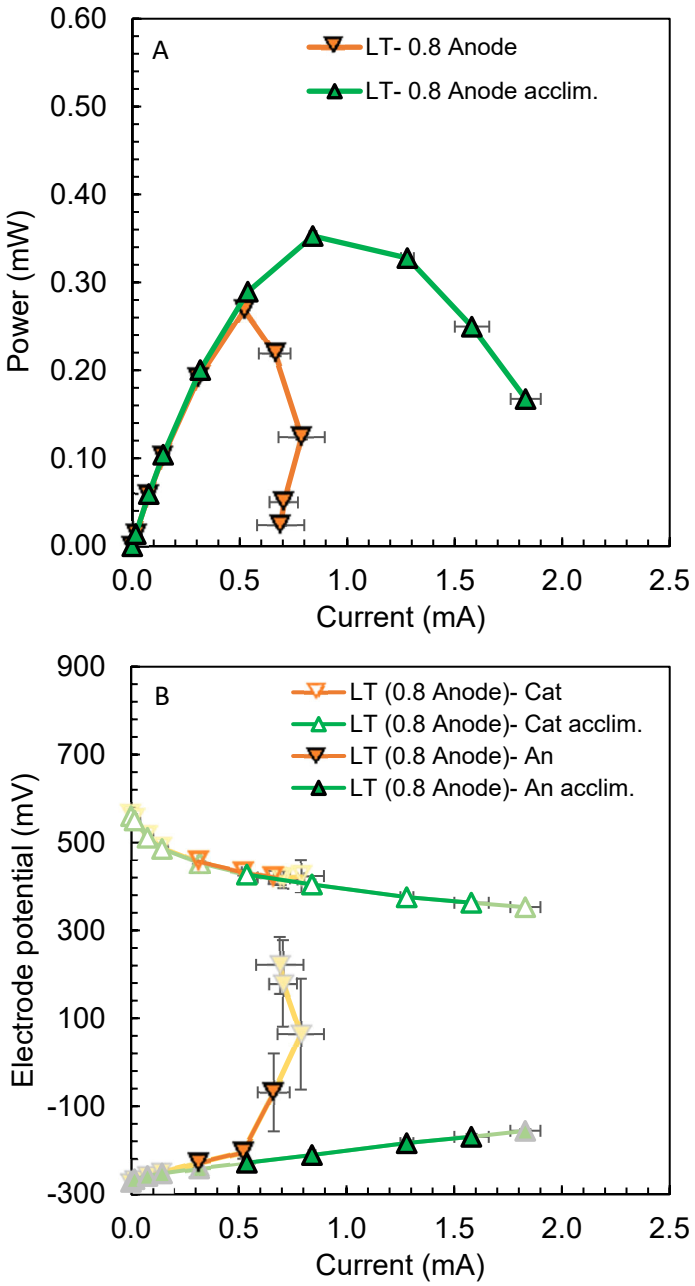

Figure S7. (A) Power and (B) electrode potentials not including solution resistance (R_{Ω}) of MFCs with 4.5 cm^2 tube area (LT) and anode projected area of 0.8 cm^2 before and after additional acclimation at low external resistance. The thick solid lines show the linearized portion of the slopes that are used to calculate the anode (R_{An}) and cathode (R_{Cat}) resistances.

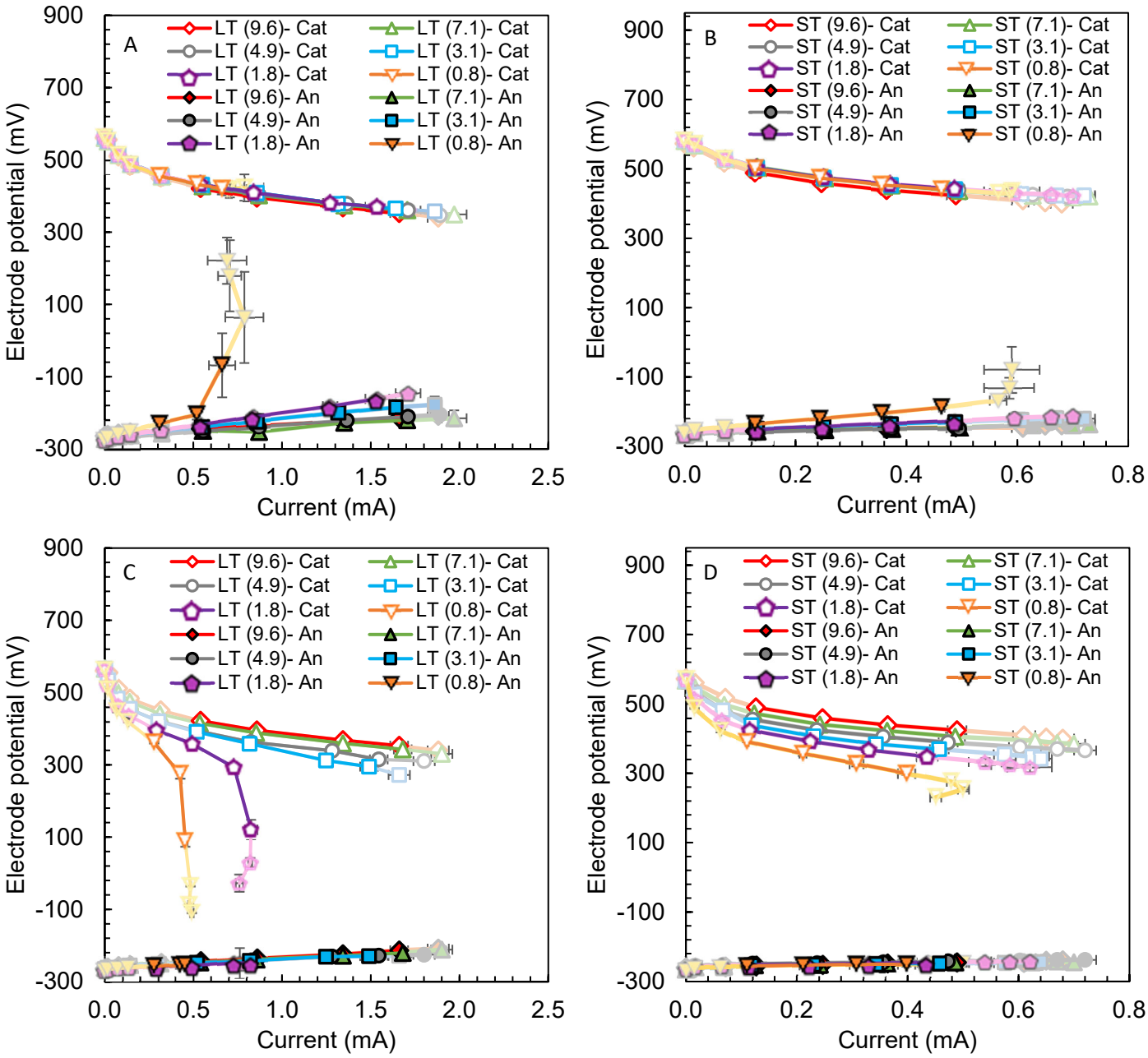

Figure S8. Electrode potentials not including solution resistance (R_{Ω}) of MFCs with 4.5 cm^2 tube (LT) and 1.2 cm^2 tube (ST) and variable (A, B) anode projected areas (from 9.6 cm^2 to 0.8 cm^2) and (C, D) cathode projected areas (from 9.6 cm^2 to 0.8 cm^2). Anode and cathode potentials including ohmic losses are reported in the Supporting information. The thick solid lines show the linearized portion of the slopes that are used to calculate the anode (R_{An}) and cathode (R_{Cat}) resistances.

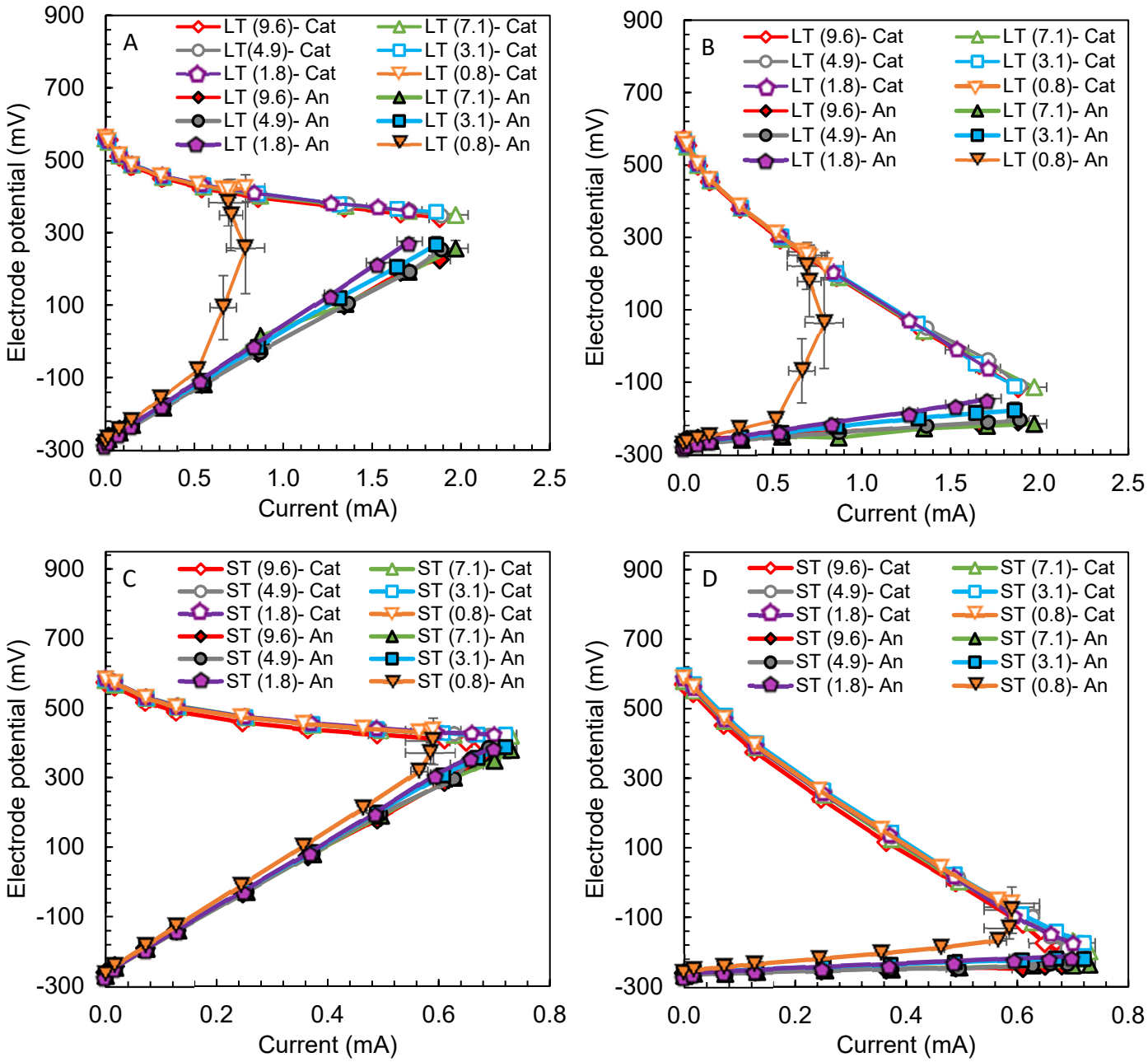

Figure S9. Electrode potentials measured in (A, B) large tube MFC (LT- 4.5 cm^2) and (C, D) small tube MFCs (ST- 1.2 cm^2) using only the reference electrode in the (A, C) cathode chamber and (B, D) anode chamber, including solution resistance (R_Ω) with variable anode projected area, from 9.6 cm^2 to 0.8 cm^2.

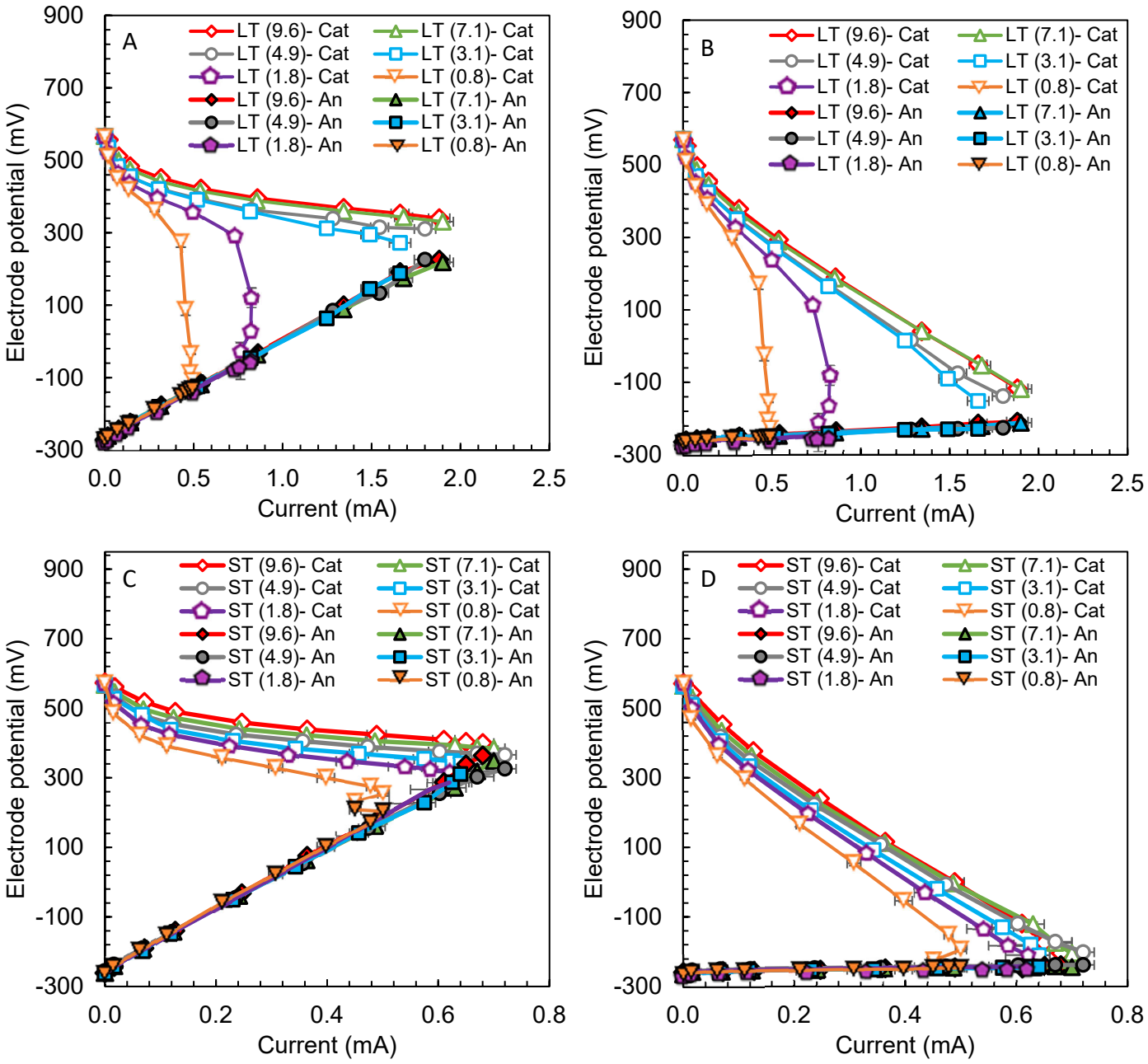

Figure S10. Electrode potentials measured in (A, B) large tube (LT- 4.5 cm^2) and (C, D) small tube MFCs (ST- 1.2 cm^2) using only the reference electrode in the (A, C) cathode chamber (RE_{Cat}) and (B, D) anode chamber (RE_{An}), thus including solution resistance (R_{Ω}) with variable anode projected area, from 9.6 cm^2 to 0.8 cm^2.

EPS analysis and current. The solution resistance of the ST-MFC was 3× that of the LT-MFC (860 Ω, SM-MFC; 258 Ω, LT-MFC), increasing the internal resistance of the cell with the small membrane and reducing the current output at the same external resistance. This shifted the electrode potentials closer to their open circuit potentials (Figure S11), likely increasing the contribution of the activation losses in the cathode resistance. For example, R_{Cat} in LT-MFC, measured from 0.54 ± 0.00 mA to 1.66 ± 0.05 mA, was 61 ± 5 Ω. In the ST-MFC, due to a different current range of currents where P_{max} occured (from 0.13 ± 0.00 mA to 0.49 ± 0.02 mA), R_{Cat} increased to 181 ± 22 Ω, even though the cathode potential showed a very similar behavior in the ST-MFC and in the LT-MFC (Figure S11).

The anode resistance was not affected by the current range selected to calculate it. For example, R_{An} was 26 ± 1 Ω in the LT-MFC and 26.5 ± 0.8 in the ST-MFC, independently of the current range, thus, the impact of activation losses on the anodic reaction is limited.

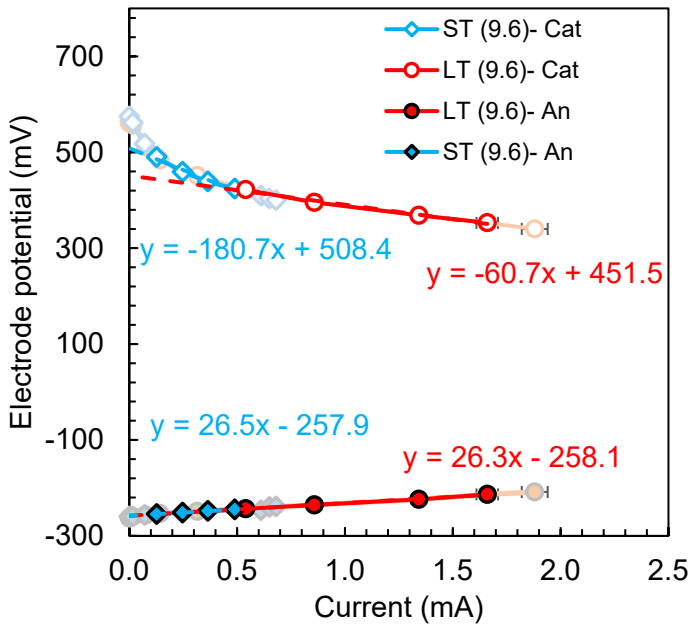

Figure S11. Electrode potentials measured in large tube (LT- 4.5 cm^2) and small tube MFCs (ST- 1.2 cm^2) with electrode areas of 9.6 cm^2.

Impact of moving the electrodes on the MFC performance. Increasing or reducing the electrode spacing by moving the electrodes in the bottles did not impact the MFC performance (Figure S12). Reducing the electrode spacing from 14 cm to 7.5 cm (length of the tube) decreased the internal resistance of only 9 Ω in the LT-MFC and 6 Ω in the ST-MFC. Increasing the distance between the electrodes by 43% from 14 cm to 20 cm by moving the electrodes on the opposite side of the bottle increased the internal resistance of 20 Ω in the LT-MFC and 5 Ω in the ST-MFC, impacting the solution resistance by less than 8% in LT-MFC and 0.7% in the ST-MFC.

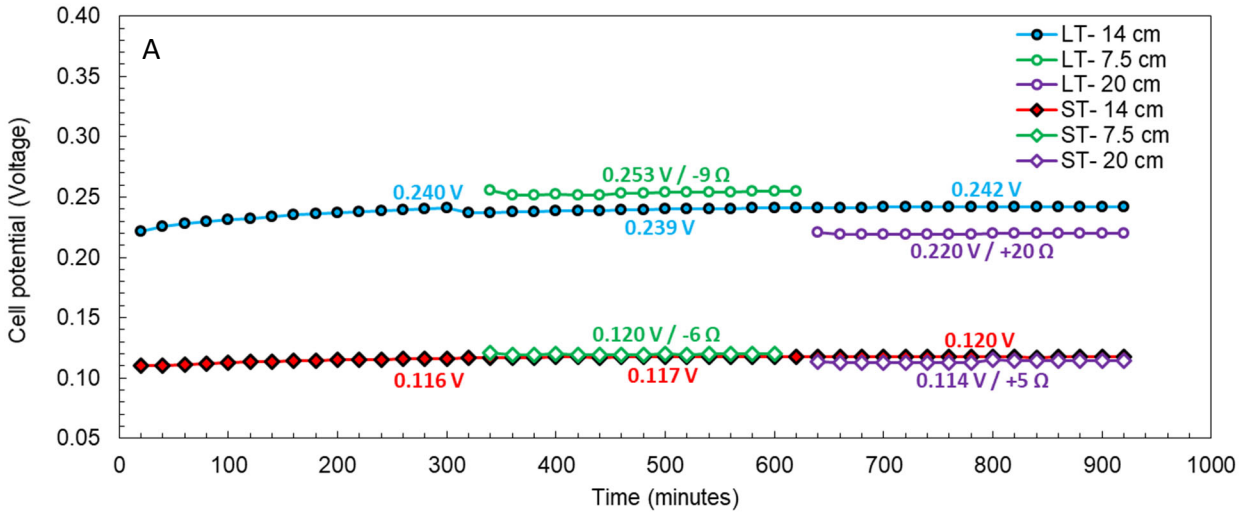

Figure S12. (A) Cell potential measured in the large (LT) and small (ST) MFCs with an electrode spacing of 14 cm, 7.5 cm and 20 cm. (B-E) Photos of the LT- MFCs with an electrode spacing of 14 cm, 7.5 cm and 20 cm.

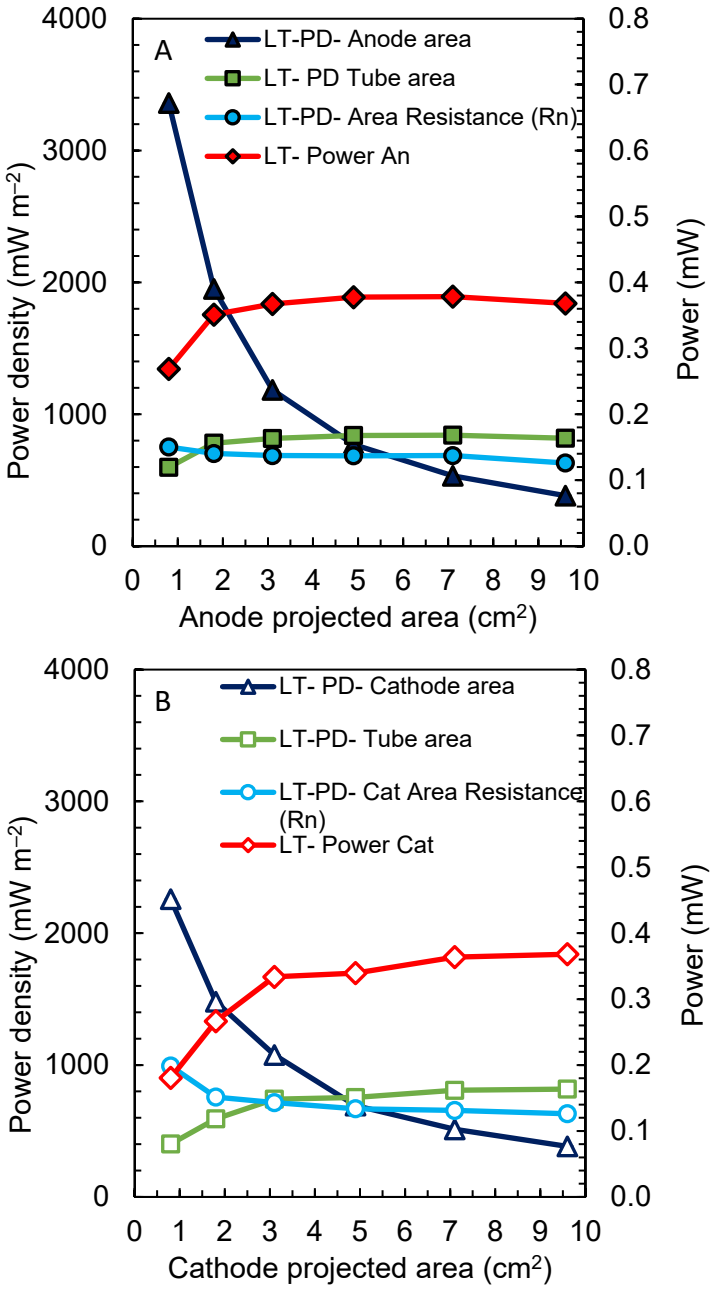

Figure S13. Maximum power (P) and maximum power density (PD) produced by the MFCs by varying the (A) anode or (B) cathode projected area normalized by the smaller electrode area, by the area-normalized resistance (R_n) or by the tube area.

Power as a function of electrode resistance and experimental potential. The MFC can be modeled as an electrochemical system comprising a voltage generator in series with the internal resistance (R_{int}). The potential is represented by the difference between the operative cathode and anode potentials ($E_{Cat,e0}$; $E_{An,e0}$) while the internal resistance is the sum of the solution (R_{Ω}), anode (R_{An}), cathode (R_{Cat}) and membrane (R_{mem}) resistances.[9,10] Each of these parameters can be obtained through the EPS analysis and by modelling this system with variable external resistances is possible to reproduce the power production by MFCs (Figure S12). The analysis of the specific resistances and electrode potentials and their impact on the total performance will allow evaluating specific improvement independently by the overall MFC configuration.

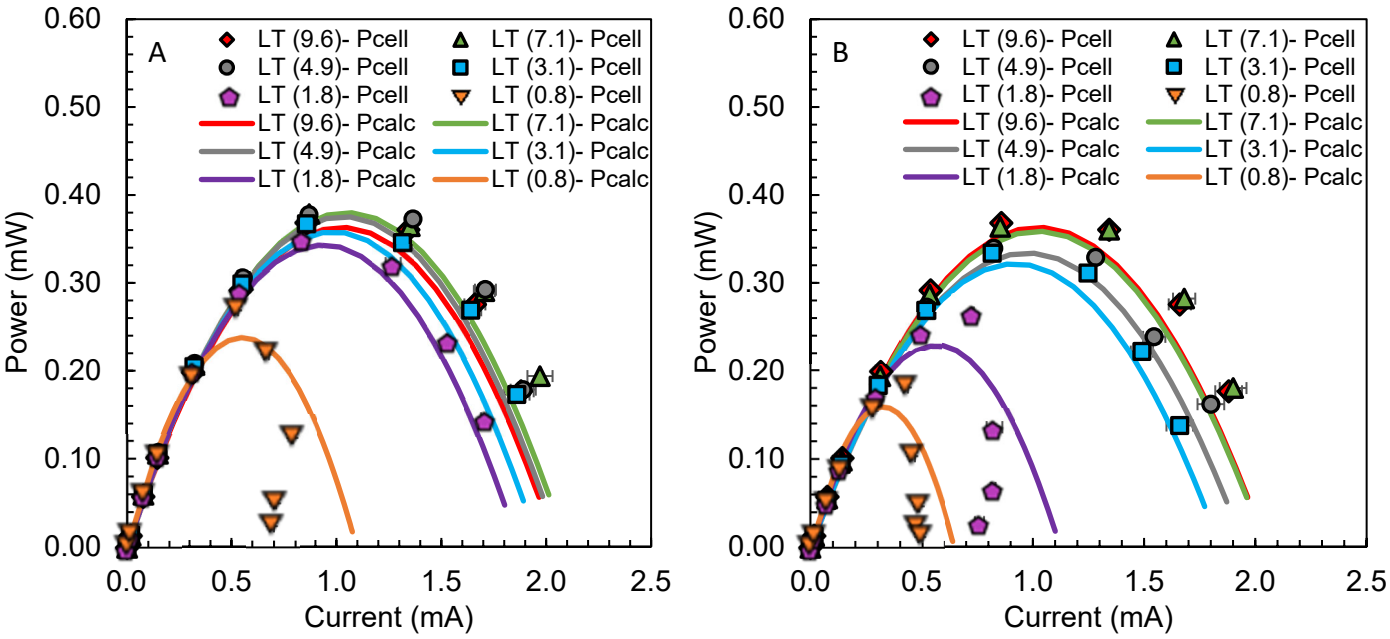

Figure S14. Comparison of the power produced in LT-MFC (4.5 cm^2) and the power curve modeled (P_{model}) using EPS analysis from the electrode specific resistances and potentials with (A) variable anode and (B) variable cathode areas.

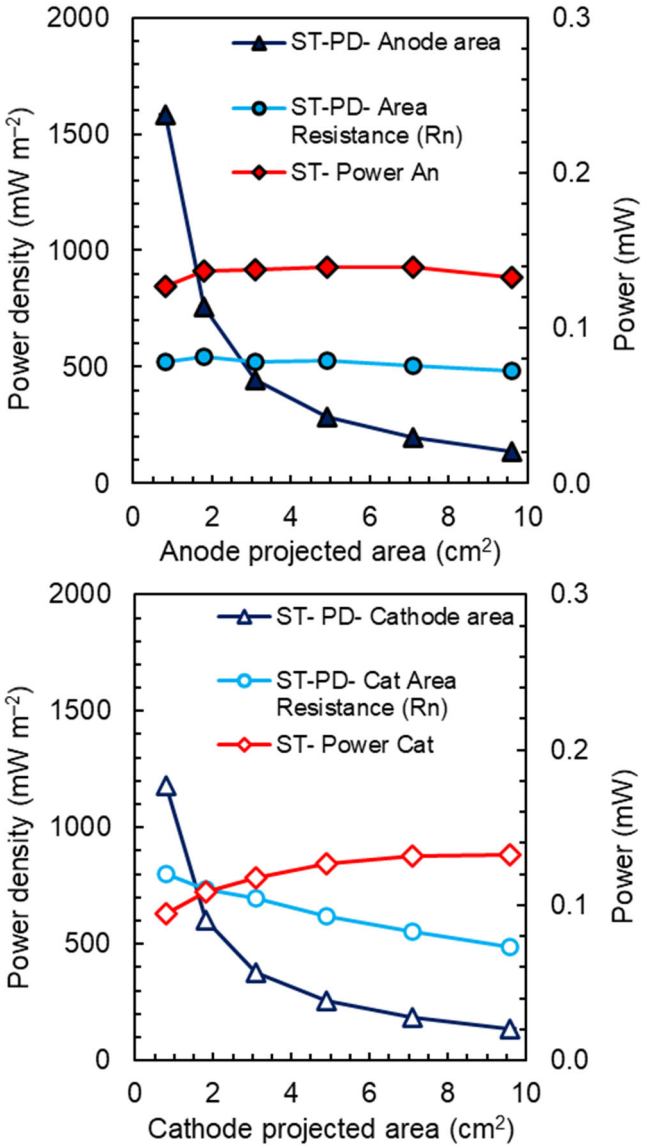

Figure S15. Maximum power (P) and maximum power density (PD) produced by the ST-MFCs by varying the (A) anode or (B) cathode projected area normalized by the smaller electrode area or by the area-normalized resistance.

References

[1] S. Ahn, B.J. Tatarchuk, Air electrode: identification of intraelectrode rate phenomena via AC impedance, J. Electrochem. Soc. 142 (2006) 4169. doi:10.1149/1.2048480.

[2] F. Alcaide, E. Brillas, P.L. Cabot, EIS analysis of hydroperoxide ion generation in an uncatalyzed oxygen-diffusion cathode, J. Electroanal. Chem. 547 (2003) 61–73. doi:10.1016/S0022-0728(03)00190-6.

[3] A. ter Heijne, D. Liu, M. Sulonen, T. Sleutels, F. Fabregat-Santiago, Quantification of bio-anode capacitance in bioelectrochemical systems using Electrochemical Impedance Spectroscopy, J. Power Sources. 400 (2018) 533–538. doi:10.1016/j.jpowsour.2018.08.003.

[4] X. Dominguez-Benetton, S. Sevda, K. Vanbroekhoven, D. Pant, The accurate use of impedance analysis for the study of microbial electrochemical systems, Chem. Soc. Rev. 41 (2012) 7228–7246. doi:10.1039/c2cs35026b.

[5] B. Hirschorn, M.E. Orazem, B. Tribollet, V. Vivier, I. Frateur, M. Musiani, Determination of effective capacitance and film thickness from constant-phase-element parameters, Electrochim. Acta. 55 (2010) 6218–6227. doi:10.1016/j.electacta.2009.10.065.

[6] G.J. Brug, A.L.G. van den Eeden, M. Sluyters-Rehbach, J.H. Sluyters, The analysis of electrode impedances complicated by the presence of a constant phase element, J. Electroanal. Chem. 176 (1984) 275–295. doi:10.1016/S0022-0728(84)80324-1.

[7] A. Lasia, Electrochemical impedance spectroscopy and its applications, Springer, New York Heidelberg Dordrecht London, 2014. doi:10.1007/978-1-4614-8933-7.

[8] M.E. Orazem, B. Tribollet, Electrochemical Impedance Spectroscopy, 2008th ed., John Wiley & Sons, Inc.,Publication, Hoboken, New Jersey, 2008.

[9] B.P. Cario, R. Rossi, K.Y. Kim, B.E. Logan, Applying the electrode potential slope method as a tool to quantitatively evaluate the performance of individual microbial electrolysis cell components, Bioresour. Technol. 287 (2019) 121418. doi:10.1016/j.biortech.2019.121418.

[10] R. Rossi, B.P. Cario, C. Santoro, W. Yang, P.E. Saikaly, B.E. Logan, Evaluation of electrode and solution area-based resistances enables quantitative comparisons of factors impacting microbial fuel cell performance, Environ. Sci. Technol. 53 (2019) 3977–3986. doi:10.1021/acs.est.8b06004.